Earthquake Geotechnical Engineering for Protection and Development of Environment and Constructions – Silvestri & Moraci (Eds)
© 2019 Associazione Geotecnica Italiana, Rome, Italy, ISBN 978-0-367-14328-2

Seismic strength capacity of gravelly backfill reinforced with geocells in retaining walls evaluated by shaking table tests

H. Munoz & T. Kiyota
Institute of Industrial Science, University of Tokyo, Tokyo, Japan

ABSTRACT: The seismic performance of a series of geosynthetics reinforced soil retaining walls (GRS RW), comprising of poorly graded gravel reinforced with geocell layers, was studied by shaking table experiments conducted on models. Geocell layers, unlike planar geogrid conventionally used to tensile-reinforce the backfill of a GRS RW, are able to accommodate a wide range of gravel sizes within their cells. This feature becomes advantageous to backfilling a GRS RW with large-size poorly graded soil. The positive effects of the three dimensional feature of the geocell on the backfill strength and backfill stiffness were also analysed. Furthermore, the failure mechanisms of the GRS RW models are outlined via 3D Digital Image Correlation analysis. On the above premise, it was found that geocells can tensile-reinforce effectively a GRS RW to attain high stability and so seismic performance.

1 INTRODUCTION

Geosynthetic-reinforced soils retaining walls (GRS RW) and integral bridges (GRS IB) have demonstrated to be seismically more stable structures in contrast to ordinary unreinforced soil structures when subjected to high seismic demands under cost-effective requirements (Munoz et al., 2012, Tatsuoka et al, 2014, Tatsuoka et al, 2017). GRS technology has become the standard for the design and construction of reinforced soil structures in Japan for very important (Rank I), important (Rank II) and other non-critical soil structures (Rank III).

Geogrid layers, as planar tensile reinforcements, are conventionally used to tensile-reinforce the backfill of GRS structures. Good interlocking soil-geogrid is relevant to achieve a high pull-out resistance of the reinforced soil-wall system. However, when quality soil for structural backfilling a GRS RW is not available, it is difficult to construct cost-effectively a GRS structure to meet seismic requirements. In this view, the authors and their colleagues (e.g. Kiyota et al., 2009) proposed to investigate the performance of geocells reinforcing poorly graded gravel backfill for new types of GRS RW via physical models. The present paper shows that large size gravelly soil is effectively tensile-reinforced by geocell layers which contributes to the making a sturdy structure. Image analysis of the physical models shows that the induced deformations of the backfill, and associated shear strain localisation together with the rate of strength and stiffness degradation of the backfill, are major contributors to reduction in the dynamic stability of a GRS RW system.

2 GRS RETAINING WALL MODEL

The models corresponds to the typical GRS RW prototype having a staged-constructed full-height rigid (FHR) facing. The GRS RW includes three major features: 1) staged-construction procedure to ensure the wall stability during backfilling, compaction, and wall construction before casting-in-place the FHR facing, 2) the use FHR facing where a number of reinforcement layers are firmly connected, and 3) the use of geosynthetics layer as tensile-reinforcement

material. Models of the conventional type RW and two types of FHR-facing GRS RWs were constructed (grid-reinforced model and the geocell-reinforced model).

The scaled down prototype to model followed scale similitude rules (Munoz et al, 2012, Tatsuoka et al, 2012). The models were designed considering a scale-down factor in length λ and stress of 10. The GRS RW systems tested herein have a FHR facing with reinforcements layers firmly attached to its face while the backfilled is made of poorly graded gravel. The wall model (40 cm-width×50 cm-height and 3 cm-thickness) was made of duralumin and its back face and the bottom surfaces, in direct contact with the backfill and supporting ground, were made rough by covered them with a sheet of sandpaper No. 150.

The GRS RW models were erected inside a rectangular prismatic steel box (180 cm-long × 40 cm-wide×87.5 cm-high) fixed to a shaking table. Figure 1a shows a picture of a GRS RW model mounted on the shaking table apparatus. The front and back sides of the box comprises of a transparent-tempered glass window which allowed observing the in-plane displacements and deformations of the models during the shaking events.

2.1 *Reinforcement of the backfill*

The backfill was reinforced for a region of 40 cm-width×50 cm-height and 36 cm in length. In total 10 layers of reinforcement for a width of 39.5 cm were arranged at a vertical spacing of 5 cm in the backfill. The reinforcement layers were firmly connected to the wall face by either bolts or clamps. Under this arrangement, high connection strength between the reinforcement layers and the wall face was ensured. In all the models, the backfill and supporting ground were made by dry-tamping poorly-graded gravel (D_{50}= 14.2 mm, Uc= 1.44, Gs= 2.65; maximum dry density D_{max}=1.87 g/cm^3) to a prescribed dry density of about 0.95 D_{max}=1.78 g/cm^3 (void ratio e=0.49)

Two different types of reinforcement layers were used: 1) phosphor-bronze grid of 1 mm thickness having its surface made rough by sand gluing, in order to promote grid-gravel friction. The phosphor-bronze grid has an aperture of 35 mm× 35 mm (Munoz et al. 2012), and 2) a new type of square-shaped cell mattress composed of three-dimensional cells with dimensions of 50 mm× 60 mm× 25 mm (Xinye et al, 2017). This reinforcement is made of polyester.

A series of pull-out experiments were conducted on the composite reinforcement-gravel to evaluate the extent their interactions when subjected to lateral force. Typical curves of pull-out resistance versus displacement of these reinforcements indicates that the geocell-gravel composite, exhibited the highest pull-out resistance (~7.5 kN/m) in contrast to phosphor-bronze grid (~4.5 kN/m). Therefore, it was expected the GRS RW geocell-reinforced to perform dynamically more stable in contrast to GRS RW grid-reinforced. Furthermore, neither of the reinforcements failed by tensile rupture, but by pull out. Therefore, the reinforcement models can represent high tensile-strength reinforcements used in actual construction.

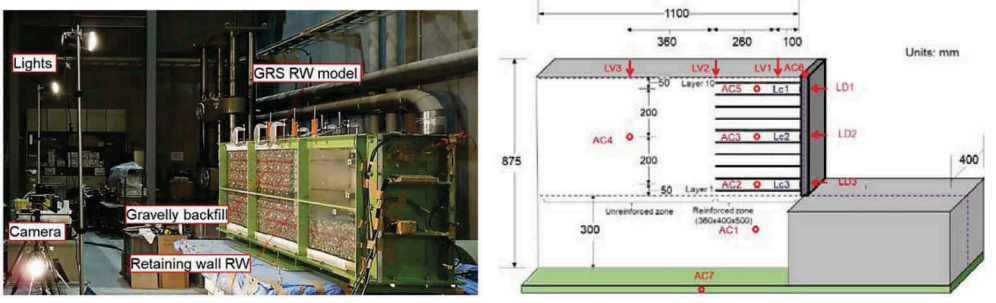

Figure 1. a) Shaking table, GRS RW model and image acquisition setup b) typical instrumentation of the models.

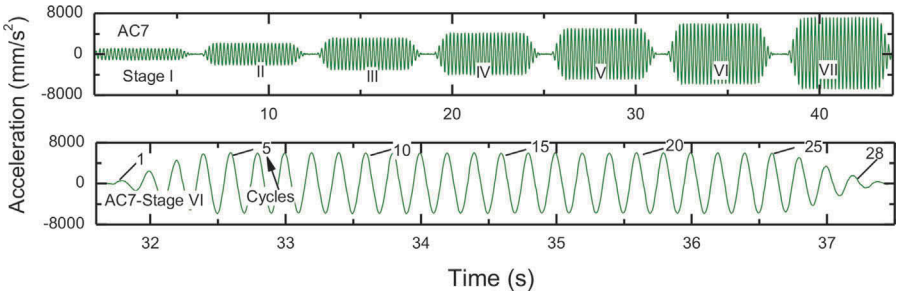

Figure 2. Typical time history of base acceleration by AC7 applied to the models.

2.2 *Instrumentation of the models*

The models were densely instrumented by contact-measurement devices at locations relevant to monitor 1) displacements by either displacement transducer LVTD (LV1 to LV3) or laser-displacement sensors (LD1 to LD3), 2) earth pressures (LC1 to LC3) and 3) accelerations. Accelerations were recorded by a set of small-size accelerometers set up on the shaking table (AC7), on the upper-top wall (AC6) and embedded within the backfill (AC2 to AC5) and foundation ground (AC1), see Figure 1b. Once the models were constructed and instrumented, they were subjected to a scale-down time history of accelerations applied to the base of a shaking table apparatus.

3 DYNAMIC LOADING ON THE MODELS

Each model was subjected to a history of sinusoidal base acceleration with twenty sinusoidal cycles during steady shaking per loading stage. This number of cyclic loading is representative of a Mw 8.0 earthquake, see (Seed et al, 1983). The base acceleration amplitude was increased about each 100 gal (1 m/s^2) per stage until failure or collapse of the structures took place. In all the model tests, the base acceleration was applied at a natural frequency, f_i equal to 5 Hz to simulate the predominant frequency of the Kobe earthquake (Munoz et al., 2012). Figure 2 shows the typical base acceleration applied to the shaking table and recorded by AC7.

In addition, a static load of 1 kPa surcharge made of lead shot bags, was placed on the crest of the backfill of the models to simulate the weight of pavement for railways or highways, assumed to be equal to 10 kPa in actual construction.

4 FIELD OF DEFORMATIONS OF THE MODELS

4.1 *Conventional type retaining wall (T-shape-G)*

Digital image correlation (DIC) provided deformations and motions of a large area of interests. This technique aids to reveal major insights into the evolution of strain localisation of geomaterials (Munoz et al. 2016a,b, 2017 a,b). Figure 3a shows the failure sequence of the model. With this model, large deformations of the wall and its backfill were observed, under relatively low seismic demands, i.e. a base acceleration about 400 gal (4 m/s^2).

Figure 3b shows the cumulative residual deformations of the backfill and foundation ground with T-shape-G model obtained by DIC analysis. This figure shows that the vertical deformations (settlements) became less than about 1 mm (less than 0.2% the height of the wall) for acceleration demands less than 300 gal (3 m/s^2), loading Stage III. Under this condition, the wall can be considered stable.

However, after increasing the applied base acceleration by about 100 gal (1 m/s^2), a demand of 400 gal (4 m/s^2), loading Stage IV, a sudden and abrupt overturning of the wall took place inducing large settlements of the backfill crest. That is, settlements, larger than 40 mm (8% the height of the wall) in a wedge in the backfill in contact with the back face of the wall. A brittle failure of the wall system took place.

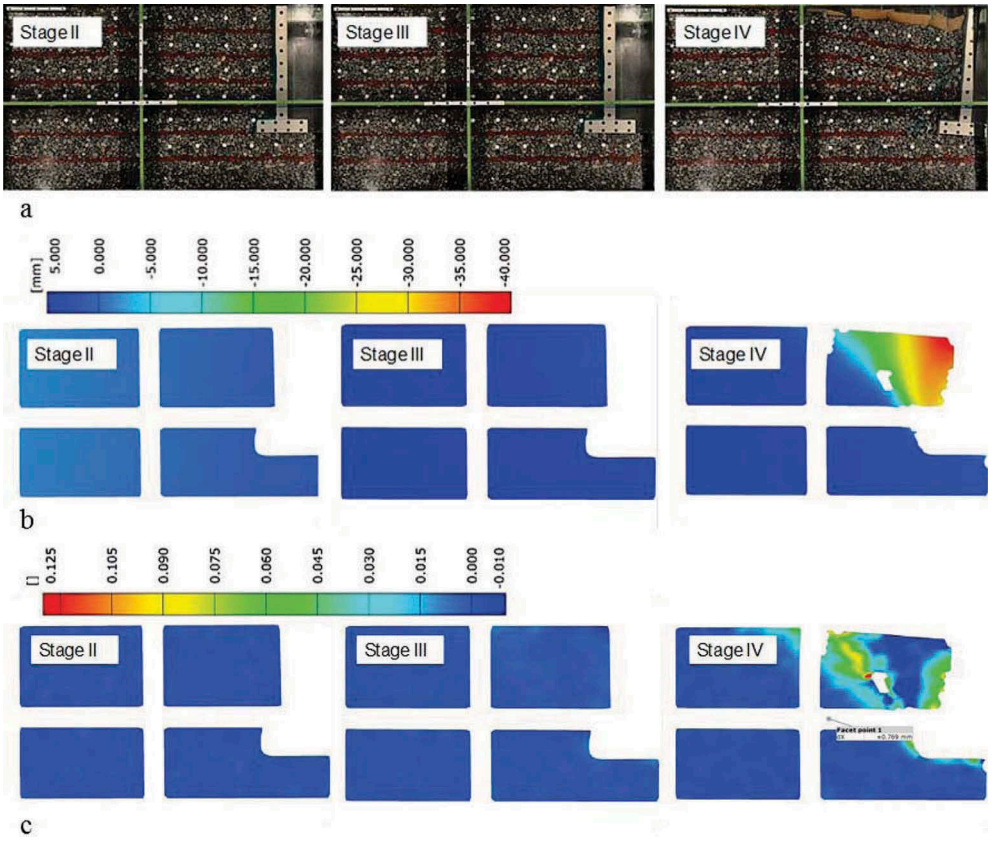

Figure 3. Failure patterns of the conventional unreinforced RW with gravel backfill at residual stages a) testing, b) settlement field and c) shear strain field.

In this manner, relatively large shear strains, up to about 10%, localised suddenly along an inclined failure plane in the backfill as the amplitude of the demand acceleration and number of loading cycles increased in Stage IV, as demonstrated in Figure 3c. In Figure 3c and subsequent figures, the shear strain values correspond to total shear strain comprising of both cyclic and average shear strain.

4.2 *GRS RW having the backfill reinforced with phosphor bronze grids (Geogrid^M-G)*

Figure 4a shows the deformation of the GRS RW model having the gravelly backfill reinforced with phosphor bronze grids subjected to 600, 700 and 800 gal (6, 7 and 8 m/s^2) of demand acceleration (only this stages are shown here for convenience). Figure 4b shows the cumulative residual vertical deformations of the wall system. This GRS RW model performed far more stable against higher seismic demands compared to the conventional unreinforced RW, i.e. the T-shape-G described above.

With Geogrid^M-G, after the end of loading Stage IV (image not shown), vertical deformations accumulated progressively in a wedge in the unreinforced backfill located immediately behind the reinforced zone block. In contrast, the reinforced zone only deformed vertically about 0.75 mm (0.15% the height of the wall).

At the end of loading Stage V (image not shown), and subsequent loading stages, the formation of a wedge in the unreinforced backfill is pronounced. This wedge formation may be attributed to the dual-ratcheting mechanism that took place in the unreinforced backfill zone. This is, the wedge formation is induced by the active and passive movements of the wall and the reinforced zone block. Maximum settlements in this wedge reached 0.5% the height of the wall.

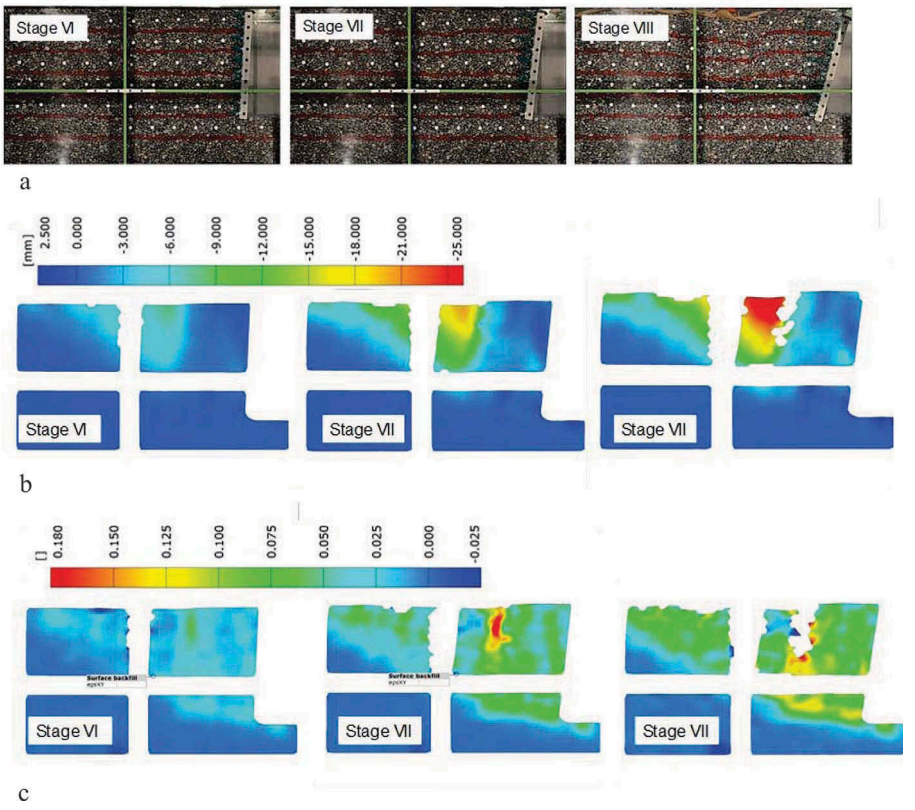

Figure 4. Failure patterns of the reinforced RW with geogrid at residual stages a) testing, b) settlement field and c) shear strain field.

As shown in Figure 4b, base acceleration of 600 gals (6 m/s^2, loading Stage VI) induced further deformations of the backfill together with displacements and rotations of the wall. Maximum settlements in the unreinforced wedge reached 1.2% and 4% the height of the wall at the residual states of loading Stages VI and VII, respectively. Only under a relatively high seismic demand in Stage VIII, about 800 gal (8 m/s^2), settlements became larger than 5% the height of the wall.

The field of shear strains in the backfill shown Figure 4c reveals that the development of shear strain did take place progressively, unlike with the case T-shape-G case where shear strain development was abruptly. The failure of the wall system was ductile.

Shear strain was negligible after the end of loading Stage IV, less than 0.3%, and no localisation of strains were observed in the backfill at this stage (image not shown). Figure 4c shows that with increasing both the amplitude of base acceleration and the number of loading cycles following Stages VI, VII and VIII, shear strains grew and localised markedly in regions 1 to 4 in the backfill. Regions 1 to 4 are presented later in Figure 6 and described in section 6 of the paper. For instance, at the end of Stage VII, shear strains develop the largest in region 1, up to about 18%, while after the end of Stage VIII, shear strains did extend to more than 18%.

4.3 *GRS RW having the backfill reinforced with geocells (Geocell^{SD}-G)*

With the GRS RW geocell model (Geocell^{SD}-G), excessive deformations of the retaining wall system were alleviated and the development of deformations was effectively delayed

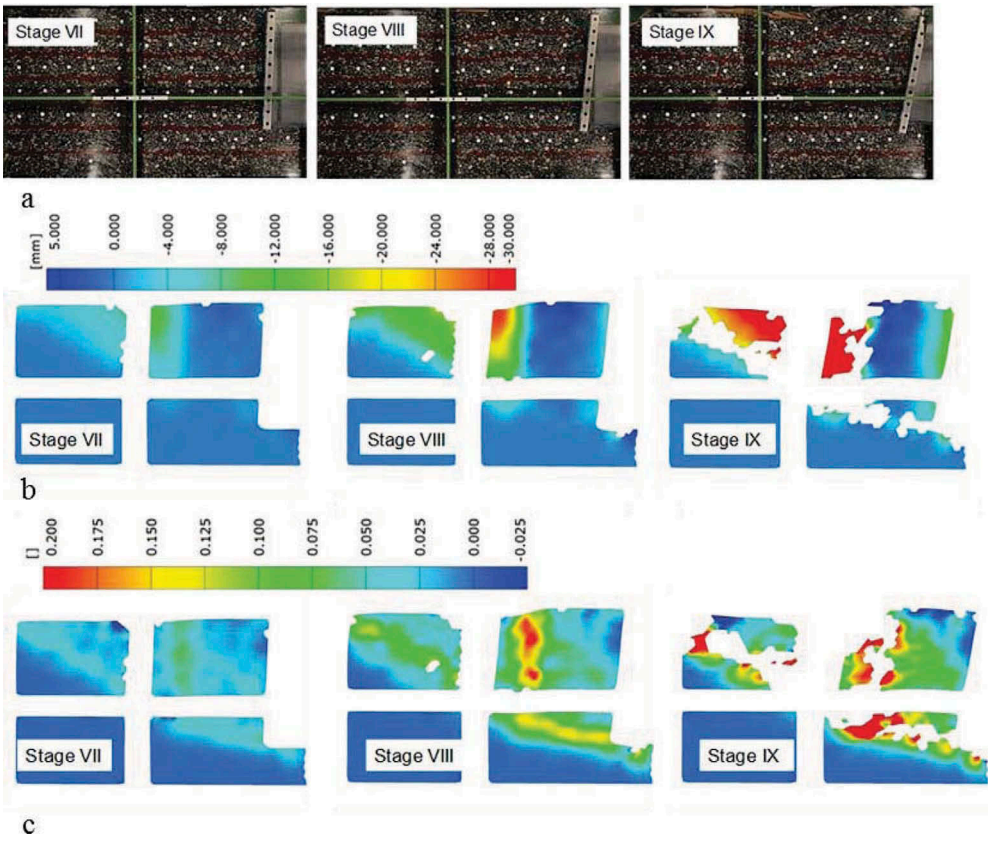

Figure 5. Failure patterns of the GeocellSD-G model at residual stages a) testing, b) settlement field and c) shear strain field.

throughout each loading stages, as demonstrated by Figure 5a, b and c. As a result, the failure and collapse of this type of wall system were reached at a loading stage under higher seismic demand, i.e. Stage IX (900 gal = 9 m/s^2). In comparison, the Geogrid^M-G model failed at Stage VII (700 gal= 7 m/s^2) and the T-shape-G model failed at Stage IV (400 gal = 4 m/s^2).

The failure of the GRS RW geocell model was ductile. Similarly, as with Geogrid^M-G, with Geocell^{SD}-G model, settlements took place the largest in the unreinforced backfill, as shown in Figure 5b.

With the GRS RW geocell model, shear strain development, and strain localisation in the backfill did take place in a lesser extent in contrast to Geogrid^M-G and T-shape-G model for the same seismic demand. For instance, at loading Stage VII, while with Geogrid^M-G model, the shear strains in the backfill are within a range of 7% to 18% (i.e. in regions 1 and 2 presented later in Figure 6), with Geocell^{SD}-G model the shear strains developed only in range 4% to 7% as shown in see Figure 5c.

At the end of loading Stage VIII, the Geogrid^M-G and Geocell^{SD}-G models show that shear strains developed in the order of 20% (region 1) in the backfill, see Figures 4c and 5c. This indicates that although Geocell^{SD}-G performed less deformable than Geogrid^M-G throughout the seismic events, the reinforcement capacity of the geocell, as well as the strength capacity of the geocell to reinforce the backfill, may have reached their limit. More investigation is required in this matter.

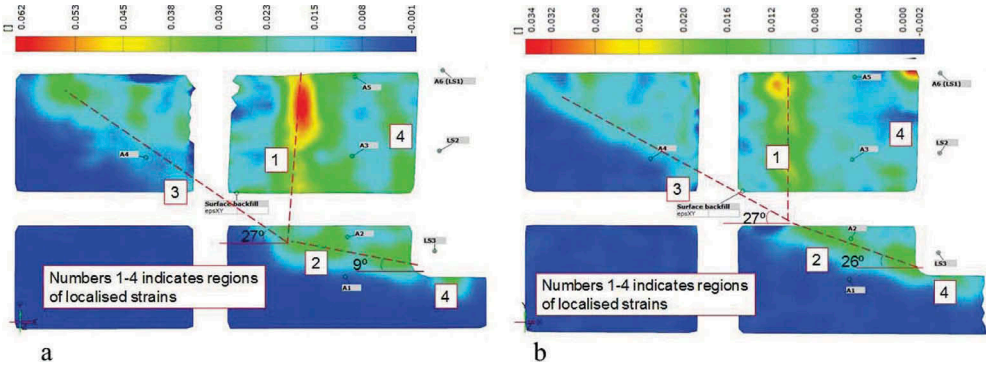

a b

Figure 6. Shear strains localised in regions 1 to 4 in a) grid and b) geocell reinforced gravel under the same base acceleration demand

5 SEISMIC PERFORMANCE OF THE MODELS

5.1 *Shear strain localisation*

In general, the FHR facing of the models experienced noticeable horizontal translations and rotation as base acceleration increased in both the number cycles and amplitude of base acceleration. At the same time, permanent deformations took place progressively at different extent within the reinforced and unreinforced zones of the backfill and foundation soil.

Shear strains developed at lower rate initially and then faster to eventually localised in the backfill and foundation soil. The results showed that shear strains localised in the following regions mainly:

1. In the backfill along the contact region between the reinforced and the unreinforced zone,
2. At the bottom in the reinforced zone, which takes the form of an inclined plane having its origin around the toe of the FHR facing and extends through the reinforced block following an inclination that depends on the reinforcement type employed,
3. In the unreinforced zone (immediately behind the reinforced zone) along an inclined plane of a wedge that was formed as a result of the repeated active and passive movements of the reinforced zone (and the wall), and
4. At interface FHR facing bottom and foundation soil. Furthermore, shear strains localised in a minor extent, at the contact in between the FHR facing and reinforced backfill.

On the other hand, locations other than 1 to 4 above experienced negligible shear strain development. This is demonstrated by the DIC analysis and results as shown in Figures 4 to 6.

5.2 *Backfill strength degradation*

The strength degradation of backfill induced by the seismic loading can be estimated by back-calculation following the study of Zeghal (Zeghal et al 1995) by integrating the equation of motions of downhole accelerometers in a soil column and using stress-free surface boundary conditions. By doing so, the time history of shear stress and shear strain can be calculated for a given soil element in a soil column. Furthermore, stress and strain relations allow for calculations of the shear modulus cycle by cycle during seismic loading.

The estimated degraded shear moduli of the considered elements at AC5, AC3 and AC2 in the backfill, and AC1 in the foundation ground is presented in Figure 7. The initial shear modulus (G_0), at strain levels of 10^{-6}, can be estimated by using Kokusho's formula (Kokusho 1981) for rounded gravel, equal to about 63 MPa for a void ratio e =0.49 and effective confinement stress on average σ_0'= 10 kPa, for the model tests.

It was found that the shear modulus reduces with the values of strain amplitude during each stage of loading as shown in Figure 7. In this respect, the rate of stiffness degradation of the

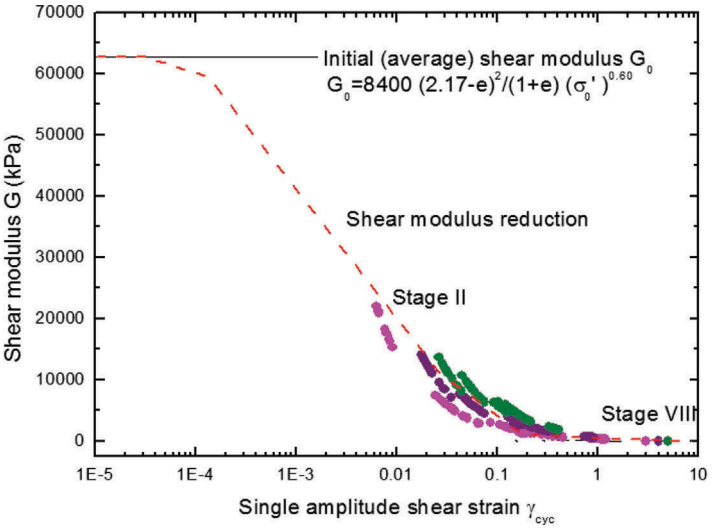

Figure 7. Stiffness degradation curves of gravelly backfill reinforced with PP geogrid from shaking table test (I, II, III, etc., represents respective loading stages)

backfill was significantly delayed due to primarily the relative stiff behaviour of the reinforced zone. However, unavoidably, due to the difference in strength and stiffness between the reinforced and unreinforced zones, large shear strains developed in the interface reinforced zone-unreinforced zone weakened the backfill greatly.

The decrease in the stiffness of the GRS RW models by degradation of its components increased the response acceleration of the backfill and the FHR facing in each loading stage which induced, and accelerated further, the degradation of the resisting components of the GRS RW models, thus accelerating the failure process.

6 CONCLUSIONS

To study the deformational patterns of geosynthetics reinforced soil (GRS) retaining walls (RW) having a full-height rigid (FHR) facing subjected to earthquake excitations, model of GRS RW having the backfill made of poorly graded gravel and reinforced with phosphor-bronze and geocell models were constructed and tested. Furthermore, their full field of deformations and strains were examined. Two-dimensional digital image correlation (DIC) method was used to do so. The field of shear strains demonstrated, for all the models, shear strains localised the largest in the backfill at the interface in between the face of reinforced zone and a wedge formed in the unreinforced zone. Shear strain development was highly alleviated when the backfill was reinforced with geocells layers. Therefore, the backfill strength was less degraded. The strength of this GRS RW was the highest compared with the typical geogrid reinforced RW type and conventional type RW.

ACKNOWLEDGEMENT

The first author would like to thank the Japan Society for the Promotion of Science (JSPS) for their financial support through the JSPS Fellowship Programme to conduct research activities at the University of Tokyo. The assistance of H Xinye, T Mera and T Katagiri from the Institute of Industrial Science, The University of Tokyo, in performing the shaking table experiments is greatly acknowledged. The authors also thank all their previous and current colleagues for their help.

REFERENCES

Kiyota T, Soma R, Munoz H, Kuroda T, Ohta J, Harata M & Tatsuoka F. 2009. Pullout behaviour of geo-cell placed as reinforcement in backfill. *Geosynthetics Engineering Journal*, 24 (1): 75-82.

Kokusho, T & Esashi, Y. 1981. Cyclic triaxial test on sand and coarse materials. *10th International Conference on Soil Mechanics and Foundation Engineering. Stockholm*. 673-676.

Munoz H, Taheri A & Chanda E. 2016a. Fracture energy-based brittleness index development and brittleness quantification by pre-peak strength parameters in rock uniaxial compression. *Rock Mechanics and Rock Engineering*, 49 (12): 4587–4606.

Munoz H, Taheri A &, Chanda E. 2017a. Local damage and progressive localisation in porous sandstone. *Rock Mechanics and Rock Engineering*, 50 (1): 3253–3259.

Munoz H, Taheri A & Chanda E. 2016b. Pre-peak and post-peak rock strain characteristics during uniaxial compression by 3D digital image correlation. *Rock Mechanics and Rock Engineering*, 49 (7): 2541–2554.

Munoz H, Taheri A &, Chanda E. 2017b. Specimen aspect ratio and progressive field strain development of sandstone under uniaxial compression by three-dimensional digital image correlation. *Journal of Rock Mechanics and Geotechnical Engineering*, 9 (1): 599-610.

Munoz H, Tatsuoka F, Hirakawa D, Nishikiori H, Soma R, Tateyama M & Watanabe K. 2012. Dynamic stability of geosynthetic-reinforced soil integral bridge. *Geosynthetics International*, 19 (1): 11-38.

Seed H B, Idriss I M & Arango I. 1983. Evaluation of liquefaction potential using field performance data. *Journal of Geotechnical Engineering*, 109 (3): 458-482.

Tatsuoka F, KosekiJ & Takahashi A. 2017. Earthquake-induced damage to earth structures and proposal for revision of their design policy—based on a case history of the 2011 off the pacific coast of Tohoku earthquake. *Journal of JSCE 5*, (1): 101-112.

Tatsuoka F, Munoz H, Kuroda T, Nishikiori H, Soma R, Kiyota T, Tateyama M & Watanabe K. 2012. Stability of existing bridges improved by structural integration and nailing. *Soils and Foundations*, 52 (3): 430–448.

Tatsuoka F, Tateyama M, KosekiJ & Yonezawa Y. 2014. Geosynthetic-reinforced soil structures for railways in Japan. *Transp. Infrastruct. Geotech*. 3-53.

Xinye H, Tomoharu M, Toshihiko K & Takashi K. 2017. Seismic response of a newly developed geocell-reinforced soil retaining wall backfilled with gravel by shaking table model test. *Geotechnical Hazards from Large Earthquakes and Heavy Rainfalls*, 513-523.

Zeghal, M., Elgamal, A-W., & Tang, H. T. 1995. Lotung downhole array. II: Evaluation of soil nonlinear properties. *Journal of Geotechnical Engineering*, ASCE 121 (4): 363-378.